JVSTB Journal of Vacuum Science & Technology B

Design of a parallel mass spectrometer for focused ion beam columns

A. Khursheed, K. H. Cheong, and H. Q. Hoang

Citation: Journal of Vacuum Science & Technology B **28**, C6F10 (2010); doi: 10.1116/1.3497021
View online: http://dx.doi.org/10.1116/1.3497021
View Table of Contents: http://scitation.aip.org/content/avs/journal/jvstb/28/6?ver=pdfcov
Published by the AVS: Science & Technology of Materials, Interfaces, and Processing

Design of a parallel mass spectrometer for focused ion beam columns

A. Khursheed,[a] K. H. Cheong, and H. Q. Hoang
Department of Electrical and Computer Engineering, National University of Singapore, 4 Engineering Drive 3, Singapore 117576

(Received 9 July 2010; accepted 16 August 2010; published 21 October 2010)

This article describes a parallel mass spectrometer design suitable for use as an add-on attachment for focused ion beam instruments. It consists of an acceleration transfer lens, an electric sector deflector, and a variable field strength magnetic sector deflector. The magnetic sector is designed to deflect and focus ions having a wide range of charge-to-mass ratios onto a flat plate detector. The size of an aperture inside the acceleration transfer lens can be used to change the spectrometer mass resolution. The simulation results presented in this article predict that it should be possible to perform secondary ion mass spectroscopy analysis on the nanoscale range with the proposed mass spectrometer attachment. © *2010 American Vacuum Society.* [DOI: 10.1116/1.3497021]

I. INTRODUCTION

The possibility of combining focused ion beam (FIB) columns with secondary ion mass spectrometry (SIMS) techniques has many potential benefits for the nanofabrication of semiconductor devices. The relatively high probe resolution of FIBs (compared to conventional SIMS instruments), if combined with SIMS analysis, will enable it to gather material information on the nanoscale, a useful companion to its milling/deposition capability. This possibility is brought closer by a recent success with techniques that implant the specimen with reactive species such as oxygen and/or cesium or use oxygen flooding, increasing the FIB-SIMS yield by over two orders of magnitude.[1] Another important step toward this goal is to design a suitable mass spectrometer attachment, one that is small enough to fit within the FIB specimen chamber. The following work presents a mass spectrometer design suitable for this purpose.

The simulations carried out in this article were done primarily through the use of numerical field distribution software and ray tracing integration routines written by Khursheed, details of which are given elsewhere,[2] and Lorentz-2EM.[3] The finite-element method was primarily used to solve for magnetic field distributions, while Lorentz-2EM was used to simulate an electric field deflector. Fourth-order Runge–Kutta techniques were used to plot trajectory paths of charged particles through all field distributions. Simulation parameters, such as the size of a numerical mesh or trajectory step, were systematically adjusted in order to minimize the influence of numerical errors on important optical parameters, such as spectrometer energy dispersion, trace-width, and mass resolution.

Normally, the magnetic deflection field strength inside magnetic sector spectrometers is constant. However, by allowing the deflection field strength to increase in the path of incoming electrons/ions, charged particles having a wide range of different energies/masses can be deflected and focused simultaneously. Figure 1 shows simulated trajectory ray paths for a beam of negative ions traveling through an asymmetric Gaussian deflection field function, $B_{z0}(x,y)$, one that is described by the following equation:

$$B_{z0}(x,y) \approx B_0 \exp\left[-\left(\frac{x-x_0}{\sigma_x(x)}\right)^2 - \left(\frac{y-y_0}{\sigma_y(y)}\right)^2\right], \quad (1)$$

where x_0 and y_0 are the x and y coordinates that define the position of the maximum field strength B_0, and $\sigma_x(x)$ and $\sigma_y(y)$ are standard deviations that describe how the function falls on either side of the maximum field strength point in the x and y directions, respectively. Ions are deflected in the x-y plane, and the magnetic deflection field is applied in the z-direction. Table I gives the field parameters required to generate the magnetic field distribution shown in Fig. 1, where the outer boundaries of the spectrometer are defined by $x_1 < x < x_2$ and $y_1 < y < y_2$ in the x-y plane.

II. GAUSSIAN FIELD BOX ANALYZER DESIGN

There are many ways to create the required magnetic field distribution for the Gaussian field analyzer. One approach is to use permanent magnets placed behind iron plates inside an iron box, as shown in Fig. 2. The strength of each pair of permanent magnets is progressively increased in the x-direction, modeled here in terms of increasing magnetic

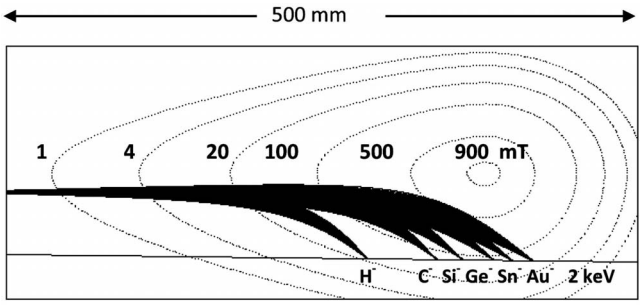

FIG. 1. Simulated ion trajectories through an analytical asymmetric Gaussian magnetic field distribution. The source is located 5 cm from the left hand edge of the diagram; ions have an energy of 2 keV and an angular spread of ±25 mrad. The dotted lines indicate contours of equal magnetic field strength (pointing normal to the page).

[a]Author to whom correspondence should be addressed; electronic mail: eleka@nus.edu.sg.

TABLE I. Parameters in Eq. (1) for analytical field distribution depicted in Fig. 1.

$B_0=0.95$ T, $x_0=380$ mm, $y_0=100$ mm
$\sigma_x(x)=47.5$ mm for $x_0<x<x_2$,
$\sigma_x(x)=\sigma_{x0}[1+0.2(x_0-x)/\sigma_{x0}]$ for $x_1<x<x_0$, where $\sigma_{x0}=62.5$ mm,
$\sigma_y(y)=36.25$ mm for $y_1<y<y_0$, and $\sigma_y(y)=36.25$ mm for $y_0<y<y_2$.

scalar potential magnitudes. Figure 3 shows simulated 2 keV ion trajectories of positive and negative ions through the Gaussian field analyzer box design, predicting that they can be simultaneously focused on to a horizontal detector. The ion source, in this case, is located at the left hand side of the box.

An indication of how well ions can be focused by the Gaussian field box analyzer design is shown in Fig. 4, which presents an estimate of the mass resolution limited by a spherical aberration, as a function of relative atomic mass. This graph was obtained by monitoring the trace-width created by angular dispersion and by comparing it with the change in distance created by mass dispersion. The mass resolution is taken to be half the total trace-width. It should be noted that Fig. 4 displays the intrinsic mass resolution and not the mass resolution projected onto the horizontal detection plane. The ion source, not shown in Fig. 4, is located outside the box spectrometer, 1 cm from the left hand side of the outer box. For the most part, the calculated mass resolution goes down by around a factor of 4 as the angular spread changes from ±20 to ±10 mrad, indicating the presence of a second-order spherical aberration (first-order focusing optics); however, at 100 amu, it decreases by around a factor of 12, showing that at least one point, higher-order focusing can be achieved.

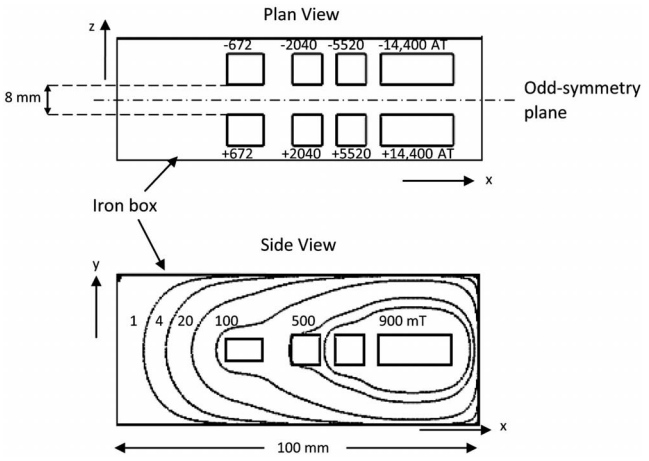

FIG. 2. Simulated field distribution simulation of the Gaussian field analyzer box. Dotted lines indicate contours of equal magnetic field strength along the central odd-symmetry plane.

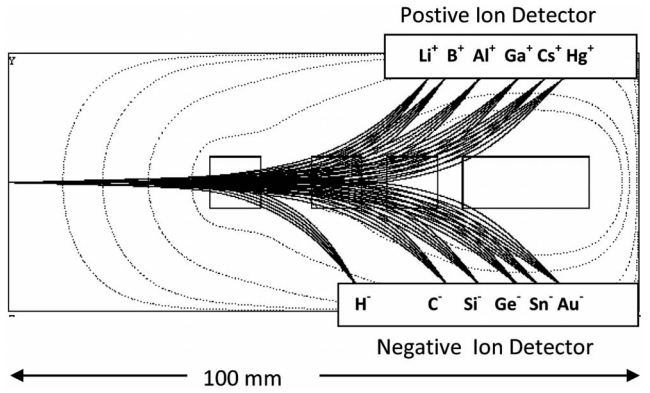

FIG. 3. Simulated 2 keV ion trajectories through the Gaussian field analyzer box design with an input angular spread ranging from −25 to 25 mrad.

III. ACCELERATION TRANSFER LENS AND ELECTRIC SECTOR DEFLECTOR

Figure 5 shows how the Gaussian field analyzer box design might be used inside a FIB specimen chamber as a mass spectrometer attachment. Ions are first extracted from the specimen by an accelerating transfer lens, which forms a cross-over point at the entrance of an electric sector deflector. The electric sector deflector is designed to compensate for the energy dispersion within the Gaussian field analyzer (to the first-order), so that the separation of ions on the detector plane comes primarily from differences in charge-to-mass ratio. Figure 6 shows simulated ion trajectories through the electric sector deflector, which has an inner radius (R_1) of 1.36 cm, an outer radius (R_2) of 2.05 cm, and an internal deflector plate voltage (V_D) of 0.597× the pass voltage (2 kV). As ions exit the electric sector, they are focused 1 cm from the left hand edge of the Gaussian field analyzer box by a three-electrode lens where the middle voltage (V_L) is set to 1.2× the pass voltage (2 kV), and the outer electrodes are set to 0 V.

Figure 7 shows the simulated electric potential distribution and trajectory ray paths for the accelerating transfer lens. A 1.2 mm aperture is used within the lens to filter out wide-angle scattered ions, so that the final exit angles lie within

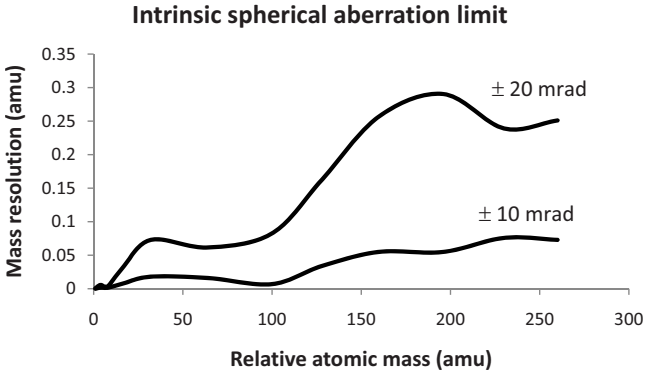

FIG. 4. Simulated mass resolution limited by an intrinsic spherical aberration as a function of relative atomic mass and angular spread for the Gaussian field box spectrometer design.

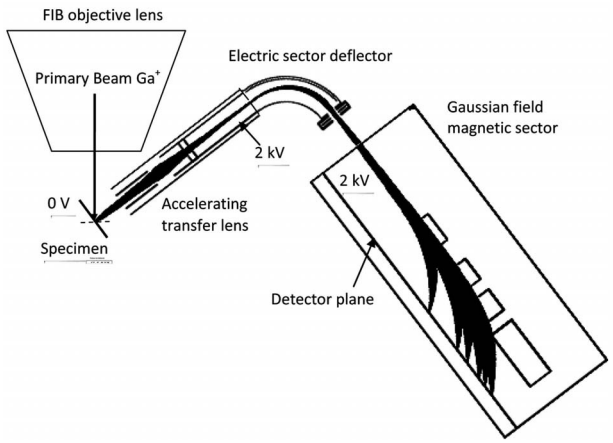

FIG. 5. FIB-SIMS mass analyzer attachment layout.

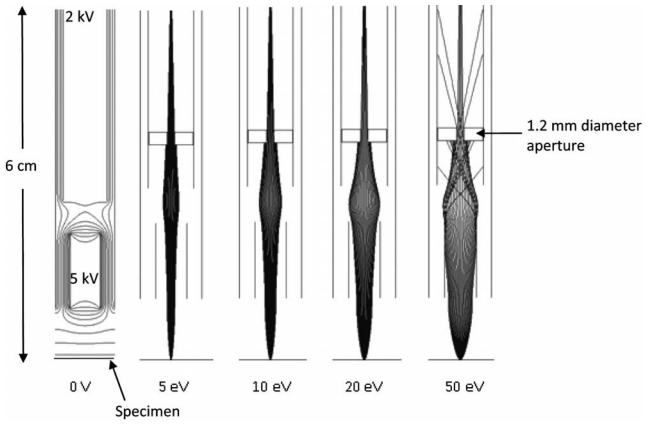

FIG. 7. Simulation of the accelerating transfer lens with a 1.2 mm diameter aperture.

±20 mrad of the central ray. This naturally reduces the transmission of scattered ions at higher emission energies. Table II presents simulation predictions of how the transmission falls with the emission energy. The transmission estimate is based upon assuming that there is a cosine polar angular distribution and comparing the number of secondary ions reaching the detector to those emitted over a small hemispherical region above the specimen. The results in Table II indicate how the aperture within the accelerating transfer lens can be used to change the energy and angular spread of the ions that reach the detector, effectively controlling the spectrometer's mass resolution.

IV. MASS RESOLUTION PREDICTIONS FOR THE GAUSSIAN FIELD BOX ANALYZER

Figures 8(a) and 8(b) present simulated mass resolution predictions limited by chromatic and spherical aberration of the Gaussian field analyzer box design. The starting positions and angles of ions at the analyzer box entrance take into account the angular/energy dispersion created by the electric sector deflector. Figure 8(a) shows that with the use of the electric sector, the predicted mass resolution due to the chromatic aberration has an average value of 0.0179 amu, two orders of magnitude better than the predicted mass resolution without the electric sector. Figure 8(b) shows the calculated mass resolution limited by the spherical aberration as it is projected onto the horizontal detector plane (not the intrinsic spherical aberration). The average mass resolution for an angular spread of ±20 mrad is 0.134 amu. These simulation results are similar to the theoretical predictions reported for other wide mass range magnetic sector spectrometer designs. For instance, in a mass spectrometer presented by Matsuda and Wollnick,[4] designed to span a mass range covering three orders of magnitude (such as the present spectrometer), a theoretical mass resolution ($M/\Delta M$) of around 10 000 is predicted for an angular spread of ±5 mrad and a relative energy spread of 0.005, which for $M=100$ amu, corresponds to a mass resolution of 0.01 amu. For the present Gaussian field box analyzer design, the simulated average mass resolution of 0.0179 amu for a relative energy spread of 0.02 (40/2000 eV) translates to 0.0044 amu assuming that the mass resolution has a linear dependence with relative energy resolution. Also, assuming that the mass resolution has a quadratic dependence with angular spread (first-order focusing and second-order spherical aberration), the predicted average mass resolution for the present spectrometer of 0.134 amu at an angular spread of ±20 mrad translates to 0.0083 amu for ±5 mrad.

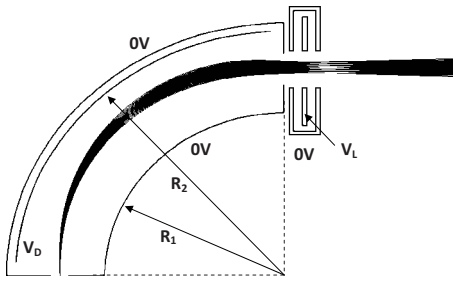

FIG. 6. Simulated ion trajectories through the electric sector designed to compensate for energy dispersion. Nine trajectories are plot in uniform steps in the angular spread range of −25 to 25 mrad, at the energies of 1940, 2000, and 2060 eV (±3% spread around the pass energy).

V. EXTRACTION FIELD EFFECT ON THE FIB PRIMARY BEAM OPTICS

The extraction electric field created by the accelerating transfer lens will naturally affect the FIB primary beam op-

TABLE II. Transmission characteristics of accelerating transfer lens for a 1.2 mm diameter aperture.

Emission energy (eV)	Emission cutoff angle (rad)	Estimated transmission (%)	Maximum exit angle (mrad)
5	0.59	30.8	20.0
10	0.4	15.1	18.9
20	0.26	6.6	16.9
50	0.13	1.7	11.2

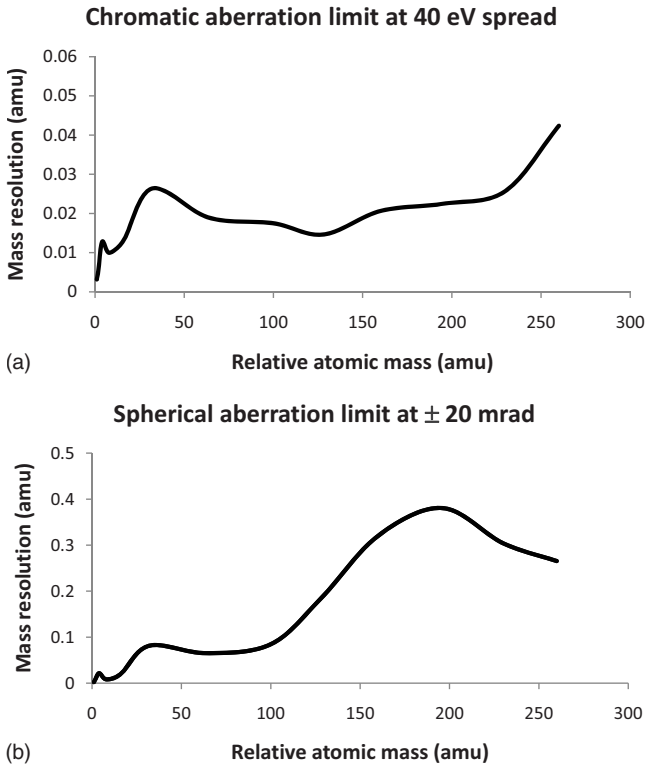

FIG. 8. Simulated mass resolution of the Gaussian field analyzer box design: (a) chromatic aberration limit at 40 eV energy spread and (b) spherical aberration limit for an angular spread of ±20 mrad.

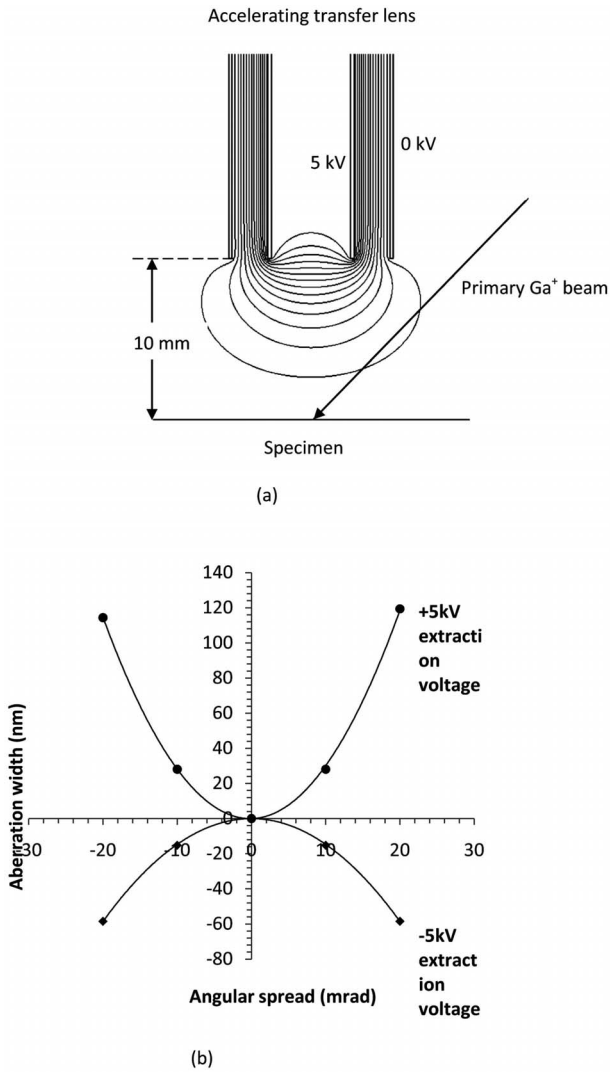

FIG. 9. Simulation of the fringe field effect created by a ± 5 kV extraction voltage on a 20 keV gallium ion primary beam: (a) simulated equipotential lines of the fringe field in uniform steps and (b) simulated trace-width at the specimen as a function of angular spread in the primary beam.

tics. To assess how significant an effect this is expected to be, direct ray tracing of a 20 keV gallium ion beam traveling through the accelerating lens fringe field was carried out for different incident angles/angular spreads. Simulated equipotentials of the accelerating transfer lens fringe field distribution are shown in Fig. 9(a). This diagram indicates that the primary beam travels through a relatively weak part of the fringe field, and therefore the effect on the primary beam is expected to be small. Simulation results based upon direct ray tracing show that the effect of the fringe field is both to displace the primary beam position along the specimen and to slightly focus/defocus it. Single rays with incident angles of 25°–60° relative to the specimen plane were plotted, and a minimum shift at the specimen ranging from 0.2 to 0.3 mm (the value depends on the sign of the extraction field) was found to occur for an incident angle of 45°. This shift at the specimen is easily compensated by deflection plates within the FIB primary beam column.

Figure 9(b) shows the simulated trace-width at the specimen as a function of angular spread around an incident angle of 45° with the angular spreads of ±10 and ±20 mrad. This is done for the extraction electrode being −5 and +5 kV (necessary to capture positive and negative secondary ions, respectively). A quadratic fit to the trace-width variation for both the extraction electrode being −5 and +5 kV was found to be adequate, indicating that the geometric (spherical) aberration caused by the fringe field is essentially second-order in nature. The angular spread of a FIB beam is usually 1 mrad or less (produced by say a 20 mm focal length objective lens and a 20 μm radius final aperture), which when projected on to the graph shown in Fig. 9(b), translates into an estimated trace-width of around 0.2 nm along the specimen plane. Since the FIB probe resolution usually lies between 5 and 20 nm, these preliminary simulation results predict that the extraction field of the accelerating transfer lens will not significantly degrade the FIB primary beam probe resolution. Therefore, these simulation results predict that it should be possible to perform SIMS analysis on the nanometer scale with the proposed FIB mass spectrometer attachment.

An important limitation of performing SIMS on the nanoscale is the inevitable reduction of the output signal strength due to the irradiation area on the specimen being smaller. If the probe size, for instance, is smaller than conventional SIMS by a factor of 10, there will naturally be 100× less secondary ions to form the output signal. For a 10 nm square area on the specimen, this may lead to only around three

useful secondary ions reaching the detector per pixel, after taking into account losses due to secondary ionization rates and spectrometer transport efficiency. Although this is an important restriction, there are some possibilities to overcome it. SIMS information is often acquired over an image, and therefore the final signal may be averaged over many similar features. This technique has been successfully applied for a Ga^+ probe of around 50 nm used to sputter Ca+ and 44 Ca+ on imaging chromosome structures; 31 chromosome samples in a single image were used to form the output signal.[5] It is also possible to use correlation methods over several images. One advantage of the present mass spectrometer design over conventional SIMS systems is that mass spectral information is to be captured in parallel, making it easier to record SIMS information in image form.

[1]D. S. McPhail, L. Li, R. J. Chater, N. Yakovlev, and H. Seng, Surf. Interface Anal. (to be published), doi: 10.1002/sia.3468.
[2]A. Khursheed, *The Finite Element Method in Charged Particle Optics* (Kluwer Academic, Boston, 1999).
[3]Lorentz-2EM, Integrated Engineering Software Inc., Canada.
[4]H. Matsuda and H. Wollnick, Int. J. Mass Spectrom. Ion Process. **91**, 19 (1989).
[5]R. Levi-Setti, K. L. Gavrilov, P. L. Strissel, and R. Strick, Appl. Surf. Sci. **231–232**, 479 (2004).